This article has been accepted for publication in a future issue of this journal, but has not been fully edited. Content may change prior to final publication. Citation information: DOI 10.1109/TSTE.2018.2834471, IEEE Transactions on Sustainable Energy

On the failure probability of offshore wind turbines in the China coastal waters due to typhoons: A case study using the OC4-DeepCwind semisubmersible

Yichao Liu, Sunwei Li, P.W. Chan, and Daoyi Chen

***Abstract*—The paper introduces a set of modelling methods to predict the failure probability of offshore wind turbines in the China coastal waters. In detail, a series of full-set three-dimensional meteorology simulations are conducted using the Weather Research and Forecast (WRF) model to provide the extreme wind fields while the extreme wave fields are predicted according to the conditional probability model. After the extreme wind and wave fields are prepared, the ultimate loads on the three critical parts of an OC4-DeepCwind semisubmersible wind turbine are simulated using the Fatigue, Aerodynamics, Structures, and Turbulence (FAST) code, which in turn leads to the prediction of the failure probability. It has been found that the OC4-DeepCwind semisubmersible constructed in the Taiwan Strait has higher chance to fail under typhoon conditions than in other parts of the China coastal waters, showing a maximum failure probability of 0.6. In addition, the failure probabilities in the South and East China Sea are in the range of 0.3-0.45. The probability densities of the ultimate loads show, in some cases, a bimodal shape, which indicates that the loads as well as the failure probability are not in a simple linear relationship with the extreme wind speeds and wave heights/periods.**

***Index Terms*—Extreme wind and wave fields; Failure probability; FAST code; Offshore wind turbine; WRF model.**

I. INTRODUCTION

The China coastal waters have been identified as suitable for the construction of offshore wind farms thanks to its ambient wind resources, high frequencies of strong wind observations and good wind power stabilities [1]. Hence, offshore wind energy exploration has been included in the national development plan and therefore is strongly supported by the government to ease the power shortage situation in megacities along the China coastline and to reduce greenhouse gas emissions [2]. Before offshore wind farms can be deployed in the China coastal areas, several technical challenges should be addressed [3]. Among the challenges, the threats posted by typhoons are our concern in the present study. It is noted that the offshore areas along the China coastline are exposed to the hazards of typhoons, who bring strong winds and waves and exert a destructive influence on the offshore wind turbine [4]. The assessment on the long-term reliability of the offshore wind turbine, which is strongly influenced by typhoons, should hence be considered in planning offshore wind farms in the China coastal waters.

It is common to assume that the long-term reliability, which is essentially the complement of the failure probability, of an offshore wind turbine can be estimated through calculating the ultimate loads under the most severe 10-min mean wind and wave conditions in a life cycle of the wind turbine [5]. Given a specific offshore wind turbine design, the limit states of three critical parts, namely the rotor blade, tower base and mooring lines, under the extreme wind-wave conditions are analyzed. Following the philosophy of the reliability analysis, Ronold and Larsen [6] proposed a probabilistic model to predict the failure of rotor blades and proved that the failure due to flapwise bending moments should be given priority in the blade design. Using the similar model, Toft and Sørensen [7, 8] have discussed the design of wind turbine blades. As for the tower base of an offshore wind turbine, Sørensen and Johansen [9] applied the probabilistic model in the estimation of the tower base failure. Based on the model, Rose et al. [10], Garciano and Koike [11] quantified the hurricane/typhoon hazards for offshore wind turbines erected off the shores of the United States and the Philippines, respectively. In addition, the failure of mooring lines has drawn attentions from scholars for various types of offshore structures [12-15], and their analysis technique could be applied to the offshore wind turbine design. Even though these published researches provide a series of reasonable methods to estimate the structural failure of offshore structures, it is still challenging to provide a reliable failure probability map of offshore wind turbines for a specified sea area. It is because a) the environmental loads acting on the offshore wind turbine are modelled purely as random variables with certain probability distributions in the previous studies. In other words, the physical natures of the loads are not included in the failure probability assessment. b) There is no systematic study, to the best of authors' knowledge, tried to put together an investigation considering different failure mechanisms systematically (failure of blades, towers and mooring system). More specifically, the published

This work was supported in part by National Natural Science Foundation of China under Grant 51608302, Shenzhen Special Funds for Future Industry Development under Grant 201411201645511650, the Economy, trade and Information Commission of Shenzhen Municipality under Grant SZHY2014-B01-001 and the Development and Reform Commission of Shenzhen Municipality under Grant DCF-2018-64.

Y. Liu, S. Li and D. Chen are with the Division of Ocean Science and Technology, Graduate School at Shenzhen, Tsinghua University, Shenzhen 518055, Guangdong, China (e-mail: liuyc14@mails.tsinghua.edu.cn; li.sunwei@sz.tsinghua.edu.cn; chen.daoyi@sz.tsinghua.edu.cn).

P.W. Chan is with Hong Kong Observatory, 134A Nathan Road, Kowloon, Hong Kong (e-mail: pwchan@hko.gov.hk).

This article has been accepted for publication in a future issue of this journal, but has not been fully edited. Content may change prior to final publication. Citation information: DOI 10.1109/TSTE.2018.2834471, IEEE Transactions on Sustainable Energy

researches generally focus on a single failure mechanism of the floating wind turbine. For instance, Rose et al. [10] quantified the failure probability of offshore wind turbines considering only the tower bending moment in the absence of ocean wave loads. Therefore, the ultimate loads on each part of the offshore wind turbine, such as the blade, the tower and the mooring lines are calculated and assessed independently. In reality, an offshore wind turbine with a floating foundation should be considered fail if one of the three critical parts fails. In such cases, the ultimate loads and the corresponding resistances in each critical part should be systematically included in a comprehensive model predicting the failure of the floating offshore wind turbine. More importantly, the probabilistic models specified for predicting the failure of offshore structures in China coastal areas have not been developed, mainly due to the lack of studies focusing on the estimation of extreme wind and wave conditions in the sea areas boarding China [16].

In order to estimate failure probabilities of floating offshore wind farms in China coastal waters, a numerical framework including a set of modelling methods is introduced. In the approach described in the present research, three major failure mechanisms, not only the tower base buckling, but also the blade root buckling and mooring line tensions are extracted from the numerical dynamics simulations and then combined to assess the failure probability of offshore wind turbines. More importantly, the extreme wind/wave loads are numerically produced based on a series of full-set meteorology simulations, which certainly show the relations between ultimate wind/wave loads and the geographic and meteorological characteristics along the coast of China.

The remainder of the paper is organized as follows. Section II briefly summarizes the numerical simulation processes, in which the modelling methods of the three-dimensional typhoon wind fields as well as the wave fields are articulated. Following the philosophy of Monte-Carlo simulations, numerical simulations are conducted to predict the ultimate loads on the three critical parts of the offshore wind turbine in section III. Through summarizing the numerical simulation results statistically, the failure probability of the offshore wind turbine is derived in section IV. Section V presents the conclusion remarks.

II. EXTREME WIND AND WAVE FIELDS

With the purpose of illustrating the modelling methods to predict the failure probability of offshore wind turbines, a flowchart has been illustrated in the Fig. 1.

As shown in the Fig. 1, three components, namely the meteorology simulation, dynamics simulation and damage model are combined in the numerical framework introduced in the present study to predict the failure probability of offshore wind turbines. It is noted that the extreme wind loads play a dominate role in predicting the failure probability of offshore wind turbines under typhoon conditions. In other words, the extreme wind speed, regarded as the critical independent variable, should be given priority in modelling the extreme loads [17]. Hence, the meteorology simulation is employed to obtain realistic typhoon wind fields while the ultimate loads on not only the tower base, but also the blade root and the mooring lines are derived from the dynamics simulation. The comprehensive failure probability including abovementioned three critical parts of offshore wind turbines using the damage model is illustrated in Fig. 1.

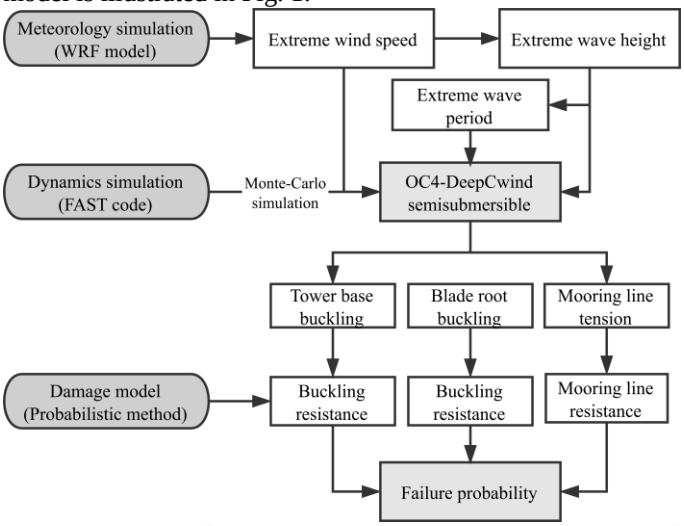

Fig. 1 Flowchart of the numerical simulation processes in terms of predicting the failure probability of offshore wind turbines.

A. Study area

In the meteorology simulation of extreme wind fields, a set of grid points covering the coastal waters with the depth varying from 20m to 1000m are established (latitudes spanning from 17°N to 40°N and longitudes spanning from 105.5°E to 125°E) with the horizontal spacing varying from 10m to 30m, to formulate the study area, as shown in Fig. 2.

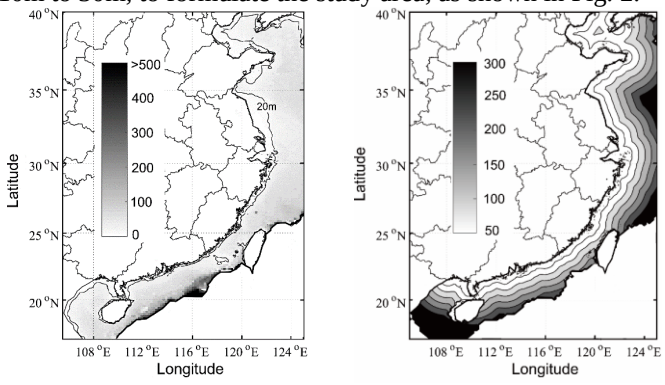

(a) (b)

Fig. 2 Calculation domain from 17°N to 40°N and from 105.5°E to 125°E. (a) Water depth (unit: m). (b) Distance from the shore (unite: km).

It is evident from the figure that the water depth varies from 20m to 200m and the distance from the shore ranges from 50km to 200km in the most parts of the study area, and hence should be considered as suitable for the deployment of semisubmersible floating wind turbines [18].

B. Extreme wind fields

1) Modelling techniques

In present study, the Weather Research and Forecast (WRF) model [19, 20], is employed to simulate a series of artificial typhoons influencing the China coastal waters. Since there is not a single historical reanalysis database containing enough environmental fields suitable for the growth of the number of typhoons planed in the present study (>1500), a modelling

method has been developed by the authors [21] to prepare the boundary and initial conditions for the artificial typhoon simulation. Following the steps articulated in the authors' previous publications, the historical reanalysis data provided by the European Centre for Medium-Range Weather Forecast[1] (ECMWF) is employed to initialize a WRF simulation, as shown in Table I.

TABLE I
DETAILS OF ECMWF HISTORICAL REANALYSIS DATA FOR WRF SIMULATIONS.

ECMWF data	Description
Time	June to October from 1979-2015 years.
3D variables	U and V component of wind, Temperature, Relative humidity and geopotential height.
26 Levels (hPa)	10, 20, 30, 50, 70, 100, 150, 200, 250, 300, 350, 400, 450, 500, 550, 600, 650, 700, 750, 800, 850, 900, 925, 950, 975, 1000
2D variables	10-meter U and V components of wind, Surface pressure, Mean sea level pressure, skin temperature, 2-meter temperature, 2-meter relative humidity.
Areas	106°E-150°E, 2°N-50°N
Resolution	0.75° ×0.75°
Interval	6 hours

In order to cover the general meteorological patterns of historical typhoons influencing China coastal waters, 37 typhoon seasons (June to October in each year) of the regional ECMWF data, whose latitude spans from 2°N to 50°N and longitude spans from 106°E and 150°E are used. According to the official descriptions for WRF model[2], the basic variables (five 3D variables at 26 pressure levels and seven 2D variables at surface level) are employed. The data is available four times at 6-hour interval a day (at 00, 06, 12, 18 UTC). In fact, Carvalho et al. [22] compared the performances of different reanalysis data in simulating the offshore winds and concluded that the ECMWF production with $0.75° \times 0.75°$ is more remarkable. Hence, following Carvalho et al. [22], the regional ECMWF data with the resolution of $0.75° \times 0.75°$ is selected for the initialization of the WRF model.

Considering the small-scale perturbations necessary for the typhoon genesis are absent due to the relatively coarse horizontal resolution of the regional ECMWF data, a three-dimensional Rankine vortex with the user-defined key parameters is inserted into the initial field as the "seed" of artificial typhoons using the numerical tool included in the WRF software package [23]. The inserted Rankine vortex is defined by the longitude and latitude of the vortex center, the radius to maximum sustainable wind speed (RMW) and the maximum sustainable wind speed. The locations and the maximum wind speeds of the artificial typhoons are drawn from the probability distributions constructed from the marginal distributions, which are produced by the best track data of historical typhoons maintained by the Hong Kong Observatory using the empirical Copula model [24], as shown in Fig. 3.

As for the RMW, it is estimated as a function of the central pressure (P_c) according to Chang et al. [25], as

$$RMW = 0.4785 \cdot P_c - 413 \quad (1)$$

[1] European Centre for Medium-Range Weather Forecasts: http://apps.ecmwf.int/datasets/data/interim-full-daily/levtype=sfc/

[2] WRF model online tutorial: http://www2.mmm.ucar.edu/wrf/OnLineTutorial/Basics/UNGRIB/ungrib_req_fields.htm

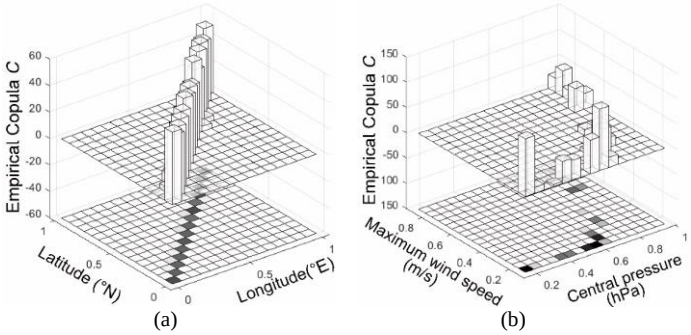

(a) (b)

Fig. 3 Joint probability distributions in relation to the marginal distributions of the (a) Location (longitude and latitude) and (b) Intensity (central pressure and maximum sustainable wind speed) of historical typhoons.

2) WRF Simulation

With the purpose of capturing the details of the three-dimensional typhoon wind fields while keeping tracks of large-scale processes, the nest-domain configuration with three inter-chained domains is employed in the WRF model. In detail, the outmost domain (D01) with fixed grid points covers the Northwestern Pacific Ocean and the coastal regions of China (latitudes spanning from 2 °N to 50 °N and longitudes spanning from 105 °E to 150 °E). The inner domains, including the intermedia (D02) and innermost (D03) domains, are configured to move with the vortex (artificial typhoon) to obtain the detailed three-dimensional wind fields. The horizontal grid spacing of D01, D02 and D03 are 27km, 9km and 3km, respectively. In the vertical direction, 39 terrain-following layers, whose vertical spacing increases with heights, as proposed by Laprise [26], are formulated to discretize the atmosphere spanning from 10hPa to 1000hPa. The physical parameterizations of the WRF model are summarized in Table II.

TABLE II
CONFIGURATIONS OF ALL THE PHYSICAL PROCESSES FOR APPLICATION OF THE WRF SOFTWARE.

Domain	D01	D02	D03
Configuration	3 nested domains (vortex following), Mercator projection		
Grid points	162 × 204	121 × 121	151 × 151
Time step	Adaptive time step (CFL≤1.6)		
Physics	Surface layer: MM5 scheme [27, 28] Boundary Layer: YSU scheme [29] Land surface model: MM5 5-layer thermal diffusion [30] Cumulus Parameterization: Kain-Fritsch scheme [31] Microphysics: WSM3 scheme [32] Radiation Physics: RRTM scheme [33] 1-D ocean mixed layer model [34]		

After the WRF settings are configured, 1510 artificial typhoons are simulated to provide the extreme wind fields. Based on the simulations of artificial typhoons, the probability distribution of extreme wind speeds is estimated. In detail, a) all the simulated typhoon wind fields are interpolated onto the pre-established grid points of the study area (Fig. 2) using the cubic spline interpolation technique [35]. b) The circular sub-region method [36] is then employed to extract the extreme wind profile at each grid point. c) Afterwards, the Generalized extreme value (GEV) distribution model [37] is employed to fit the series of the extreme wind speeds calculated corresponding to all the typhoon simulation cases at each fixed grid point using the maximum likelihood estimates (MLE) method [38]. The GEV distribution is shown as,

$$F(x|\mu,\sigma,k) = exp\left\{-\left[1+k\left(\frac{x-\mu}{\sigma}\right)\right]^{-1/k}\right\} \quad (2)$$

In equation (2), x is the extreme wind speed, k is the shape parameter, μ is the location parameter and σ is the scale parameter. All the fitted parameters at 90m level are shown in Fig. 4.

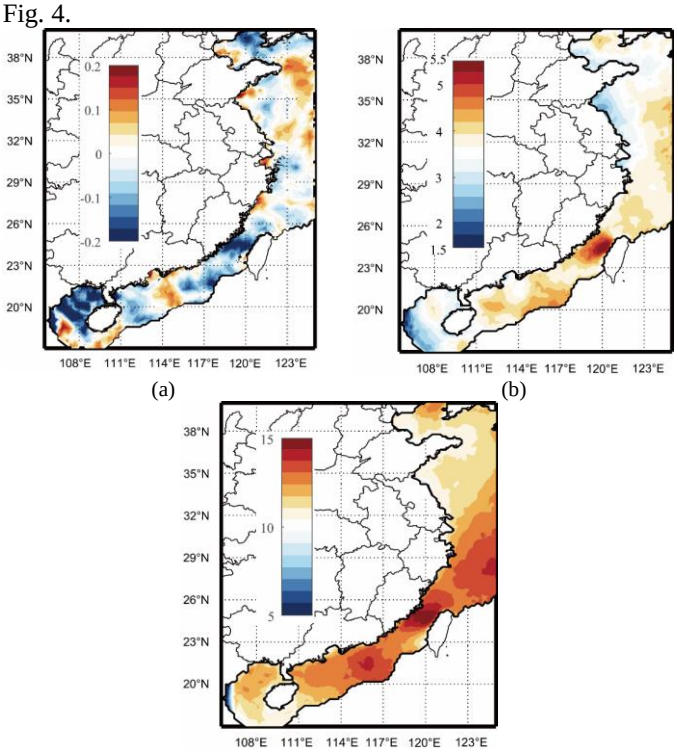

Fig. 4 Three parameters of the GEV distributions at 90m level in China coastal waters. (a) Shape parameter k. (b) Scale parameter σ. (c) Location parameter μ.

C. Extreme wave fields

Since the extreme wave fields are in connection with the extreme wind fields under typhoon conditions, the key parameters, such as the significant wave height and the spectral peak period, used to describe the evolution of wave fields could be estimated according to a conditional probability model from extreme wind speeds. According to Teng and Liu [39], who compared conditional probability models widely adopted by meteorologists to link the wind and wave fields, the log-normal distribution [40] has been found provide reasonable estimates of the key parameters defining wave fields. The log-normal model suggested by Teng and Liu [39] is shown as,

$$f(H_s|x_i) = \left[1/\left(H_s \cdot \alpha \cdot \sqrt{2\pi}\right)\right] \cdot exp\{(-1/2) \cdot [(ln(H_s) - \beta)/\alpha]\} \quad (3.a)$$

Where

$$\alpha = \sqrt{ln[(S_i/M_i)^2 + 1]}, \qquad \beta = ln\left[M_i^2/\sqrt{S_i^2 + M_i^2}\right] \quad (3.b)$$

In equation (3), H_s is the significant wave height, x_i is the wind speed at the height of 10m. When the extreme wind speed series at the height of 10m are divided into N pieces, each containing same number of extreme wind speed "samples", the auxiliary parameters α and β are calculated according to equation (3.b) from the mean (M_i) and standard deviation (S_i) of the "samples" of extreme wind speeds in the ith piece.

As for the spectral peak period, the log-normal conditional probability distribution is recommended based on the significant wave height estimated in the previous step [41], and the formula is shown as,

$$f(T_p|H_s) = \frac{1}{\sqrt{2\pi}\phi T_p} exp\left[-\frac{(lnT_p - \theta)^2}{2\phi^2}\right] \quad (4.a)$$

In equation (4.a), Θ and ϕ are the mean and the standard deviation of the logarithmic spectral peak period $ln(T_p)$, which can be estimated according to the significant wave height (H_s) as,

$$\Theta = p_1 + p_2 H_s^{p_3} \quad (4.b)$$

$$\phi^2 = q_1 + q_2 e^{q_3 H_s} \quad (4.c)$$

In equation (4.b) and (4.c), p_1, p_2, p_3, q_1, q_2 and q_3 are empirical coefficients whose values are suggested by Myrhaug and Fouques [42] based on the observations obtained via wave buoys for 29 years (from 1974 to 2002). Integrating the conditional probability distributions shown in equations (3) and (4), the probability distributions of the significant wave height and peak period can be obtained given the probability distributions of extreme wind speeds. Specifically, the probabilities of H_s and T_p can be calculated as,

$$f(H_s) = \int f(H_s|x)dF(x) \quad (5.a)$$

$$f(T_p) = \int f(T_p|H_s)dF(H_s) \quad (5.b)$$

In summary, using the GEV model predicting the probability of extreme wind speeds shown in equation (2), the probability densities of significant wave heights and wave peak periods are estimated according to equations (3)-(5).

III. Numerical Simulations

Provided vertical variations of wind speeds, significant wave heights and wave peak periods, dynamics of an offshore wind turbine can be numerically simulated via specially designed tools. In the present study, the Fatigue, Aerodynamics, Structures and Turbulence (FAST) code, which is a comprehensive aero-hydro-servo-elastic engineering simulator capable of predicting both the extreme and fatigue states of the offshore wind turbines, is employed [43].

The failure of a floating offshore wind turbine can be assessed according to the maximum bending moment at the tower base under the influence of the most severe 10-min wind climate [9]. In addition to the base bending moment, the FAST simulation also provides the ultimate loads on the blades and mooring lines of the offshore floating wind turbine, both of which are utilized to check against the resistances in the present study. In summary, the FAST code is employed to simulate the wind turbine dynamics in 10 minutes' time spans, in which the wind and wave loads are calculated based on the extreme wind speeds and extreme wave heights/periods randomly drawn from the probabilistic models derived in section II. The maximum values of blade root bending moments [6, 8], tower base buckling moment [44] and mooring line tensions [15] in each of the 10-min simulation case are the indicators assessing the failures of the blade, the tower and the mooring system.

A. OC4-DeepCwind semisubmersible

Considering that the water depth in a dominate portion of the study area (90%) varies from 20m to 200m, the semisubmersible floating wind turbine is an appealing candidate for the exploration of offshore wind resources [45]. In present study, the OC4-DeepCwind semisubmersible wind turbine [46] in accompany with the NREL 5-MW baseline wind turbine developed by the National Renewable Energy Laboratory (NREL) is employed as an example illustrating the proposed numerical framework to estimate the failure probability of offshore wind turbines. The sketches of the OC4-DeepCWind submersible are presented in Fig. 5.

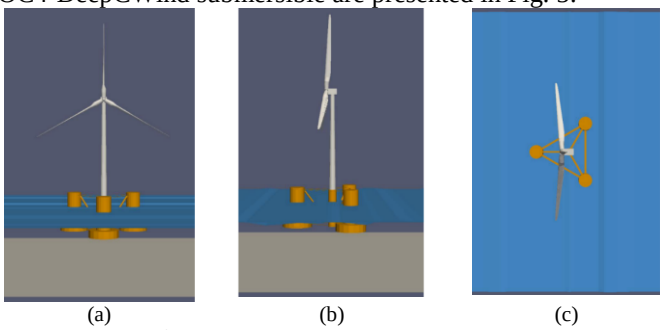

(a) (b) (c)

Fig. 5 Sketches of the OC4-DeepCwind semisubmersible wind turbine (a) Front view (b) Side view (c) Bird view.

B. Model configurations

1) Aerodynamic model

As a pre-processing tool for the aerodynamic model of the FAST system, the TurbSim software developed by NREL (version 1.06) is used to produce time series of three-dimensional turbulent wind speeds based on the extreme wind speeds at the hub height. In detail, 200 wind speed time series, each lasting 630-second, are generated corresponding to each extreme wind speed randomly drawn from the GEV model derived from fitting the WRF simulation results. The first 30-second of the time series is employed to filter out transient responses of the wind turbine. In the main simulation lasting 600 seconds, the extreme wind loads are simulated continuously at a time interval of 0.0125 seconds. Other settings used to run AeroDyn are summarized and presented in Table III.

TABLE III
DETAILED CONFIGURATIONS OF AERODYNAMIC MODULE IN FAST V8.

Aerodynamic module	Setting
Flag in AeroDyn v15.03	
Blade airfoil aerodynamics model	Steady model
Tower influence on wind around the tower	Baseline potential flow
Tower aerodynamics loads	On
Air density	1.225kg/m^3
Kinematic air viscosity	$1.464\times 10^{-5}\text{m}^2/s$
Speed of sound	335m/s

2) Hydrodynamic model

On basis of the hydrodynamic model (HydroDyn version2.03), the FAST code could calculate hydrodynamic loads on the offshore wind turbine. In the present work, the popular Joint North Sea Wave Project (JONSWAP) spectrum model [47] is employed to generate the irregular wave field. The significant wave height and the spectral peak period, which are required by HydroDyn to define the JONSWAP spectrum, are drawn from the log-normal distributions established in section II. In addition, the geophysical database[3] developed by the national oceanic atmospheric administration (NOAA) of the United States is used in the HydroDyn module to estimate the influence of water depths on wave evaluations. Parameterizations and settings used to run HydropDyn are summarized in Table IV.

TABLE IV
DETAILED CONFIGURATIONS OF HYDRODYN MODULE IN FAST V8.

HydroDyn	Setting
Water depth	The geophysical database developed by NOAA
Wave model	JONSWAP spectrum
Low cut-off frequency of the wave spectrum	0.314159
High cut-off frequency of the wave spectrum	1.570796
Significant wave height	H_s
Peak-spectral period	T_p
Peak-shape parameter	γ
Time step	0.2

3) Other models

The Mooring dynamic model (MoorDyn version 1.00.02) provided by the FAST system is employed to simulate the mooring system of the OC4-DeepCwind semisubmersible via the lumped-mass modeling approach [48], aiming to capture the nonlinear relationship between the mooring loads and the displacement of the floating platform. In order to assess the stability, the pre-tensions of the catenary lines are designed to be 25%-35% of the displacement of the floating platform, according to the American Petroleum Institute (API) code [49]. In addition to the MoorDyn, the wind turbine is set parked in the control and electrical model (SevoDyn version 1.05) to avoid the damages induced by extreme winds and waves.

When the aerodynamic loads, hydrodynamic loads, mooring loads calculated from the abovementioned modules are transmitted into the structural dynamic model (ElastoDyn version 1.03), the kinematics and dynamics of the offshore wind turbine are simulated for 10-minute simulation time.

C. Post-processing the simulation results

Using the FAST system, a total number of 200×1598 simulation cases are carried out corresponding to the 1598 fixed grid points in the study area established in section II. In the simulations, the maximum values of the three loads, namely the flapwise bending moment at the blade root (M_b), the tower base bending moment (M_t) and the mooring line tensions (T), are extracted and checked against the corresponding resistance of the turbine [7, 8, 44] using the following equation (6),

$$G(r,s) = r - s \tag{6}$$

In equation (6), r denotes the bending moment resistance of the blade root (r_b), the buckling-resistance of the tower base (r_t) and the mooring line resistance (r_m) while s is the vector of stochastic loads (M_b, M_t and T). Then the failure probability of the wind turbine is calculated as

$$P_f = P[G(r,s) \le 0] \tag{7}$$

[3] NOAA: https://www.ngdc.noaa.gov

This article has been accepted for publication in a future issue of this journal, but has not been fully edited. Content may change prior to final publication. Citation information: DOI 10.1109/TSTE.2018.2834471, IEEE Transactions on Sustainable Energy

D. Summary of verifications

Before further investigating the numerical simulation results, it is of necessity to discuss the reliability of abovementioned modelling techniques. In fact, a series of verifications have been conducted in the previous publication [21] to check the reliability of the artificial typhoon simulation, as summarized in the Table V.

In detail, the field data provided by the Hong Kong Observatory is employed to compare with not only the cumulative distribution function (CDF) of the simulated wind speeds but also the simulated mean wind profile. The error indicators of root mean square error (RMSE) and scatter index (SI) are used to quantify the agreement, as shown in the Table V.

TABLE V
SUMMARY OF VERIFICATIONS FOR ARTIFICIAL TYPHOON SIMULATION.

Verification type	Weather station	Location	RMSE (m/s)	SI (m/s)
CDF	GI station	114°06′46″E 22°17′06″N	0.85	0.098
	WGL station	114°18′12″E 22°10′56″N	0.36	0.048
	TC station	114°13′04″E 22°21′28″N	1.02	0.092
Mean wind profile	HKO station ($U_{10}=7.5m/s$)	114°10′27″E 22°18′07″N	0.36	0.048
	HKO station ($U_{10}=9.5m/s$)		0.17	0.018

The simulation results are considered as acceptable since the RMSE and SI are much lower than the error criteria in other relevant researches [50, 51]. Therefore, the simulated wind speeds yielded from the artificial typhoon simulations are reliable, even though the simulation results in the low wind speed bin (4m/s-6m/s) slightly deviate from the observed data. As for the dynamics simulation of the OC4-DeepCwind semisubmersible, the natural periods of floating foundation discerned from the free decay tests, which are regarded as the essential verification criteria, are checked after comparing with the results from a series of previous researches. In special, three degree of freedom (DOF) motion responses with an initial displacement of 3m or 3 ° are tested and the comparisons are presented in the Table VI to indicate the reliability of simulation results.

TABLE VI
SUMMARY OF VERIFICATIONS FOR DYNAMICS SIMULATION.

Research	Surge (s)	Heave (s)	Pitch (s)
Coulling et al. (FAST) [52]	107.0	17.3	26.8
Coulling et al. (Exp.) [52]	107.0	17.5	26.8
Tran and Kim (CFD) [53]	108.1	17.8	25.2
Liu et al. (CFD) [54]	107.2	17.5	27.4
The present study	110.1	17.5	25.8

It is evident from the Table VI that the comparisons of the motion period between the present study and experimental data, FAST and CFD data show acceptable agreement, even though the period of surge in the present simulation results seems to be slightly larger. In summary, not only the artificial typhoon simulation, but also the dynamics simulation process introduced in the present work is verified according to the Tables V and VI.

IV. DISCUSSIONS

A. Ultimate load maps

Based on the FAST simulation results, the mean values of the simulated ultimate loads acting on the three critical parts of the OC4-DeepCwind semisubmersible (M_b, M_t and T) are derived and presented in Fig. 6.

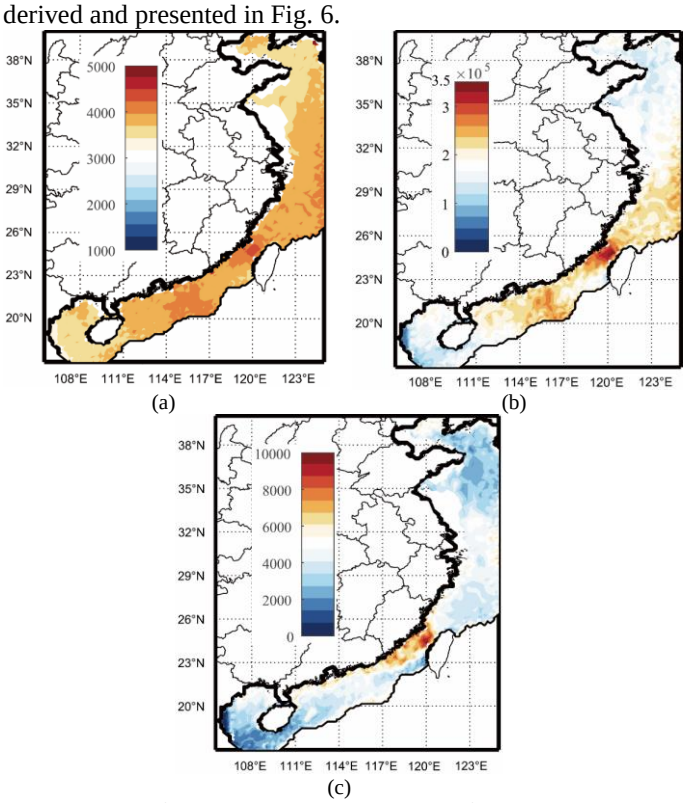

Fig. 6 Mean of the simulated ultimate loads of the OC4-DeepCwind semisubmersible wind turbine in China coastal waters. (a) M_b (unite: KN · m) (b) M_t (unite: KN · m) (c) T (unite: KN)

It is found from the Fig. 6 that the maximum ultimate loads occur in Taiwan Strait where high-valued extreme wind speeds are also observed. In fact, the ultimate loads exceed 5000KN · m, 3.5×10^5 KN · m and 10000KN respectively for M_b, M_t and T in Taiwan Strait. In addition, the ultimate loads in the South China Sea and the East China Sea are significantly larger than in other sea areas (~4000KN · m, 2.5×10^5 KN · m and 5000KN for M_b, M_t and T), implying the influences of the typhoons.

B. Area-wide failure probability

Provided the ultimate loads, the damage model (equation (7)) can be employed to estimate the failure probability. The rotor blade is currently made up of a fiber-reinforced polyester laminate in the NREL baseline wind turbine design, whose strength determines the flapwise bending resistance of blade root (r_b). Based on a series of experimental verifications [6], it is recommended that a normally distributed random variable reliably shows the statistics of r_b, whose arithmetic expectation and the coefficient of variation are $5.18\times 10^5 KN/m^2$ and 0.1 [6]. The bending stress induced by the extreme loadings at the blade root, which is compared to the resistance, is calculated as $S_b = M_b/W$, where W is the flapwise section modulus of the blade root. As for the strength

of the tower base, the buckling resistance with uncertainty (r_t) is modeled according to equation (8) [9-11, 44],

$$r_t = \frac{1}{6}\left(1 - 0.84\frac{D}{t}\frac{X_{y,ss}F_y}{X_{E,ss}E}\right)[D^3 - (D-2t)^3]X_{y,ss}X_{cr}F_y \quad (8)$$

The variables contained in equation (8) are summarized in Table VII.

TABLE VII

PARAMETERS OF RESISTANCE TO BUCKLING AT THE BASE OF A NREL 5-MW TURBINE TOWER [44]. LN=LOG-NORMAL DISTRIBUTION, COV=COEFFICIENT OF VARIANCE.

Variable	Description	Distribution type	Expected value	COV
D_{base}	Tower diameter (base)	-	6.5m	-
D_{top}	Tower diameter (top)	-	3.87m	-
t	Tower base thickness	-	0.027m	-
E	Young's modulus	LN	2.1×10^5MPa	0.02
F_y	yield stress	LN	240MPa	0.05
$X_{y,ss}$	Model uncertainties due to scale effects: yield stress	LN	1	0.05
$X_{E,ss}$	Model uncertainties due to scale effects: Young's modulus	LN	1	0.02
X_{cr}	Critical load capacity	LN	1	0.10

The resistance of the mooring line (r_m), on the other hand, can be characterized by a Weibull extreme distribution [14, 15, 55]. The arithmetic expectation of the breaking strength is empirically estimated according to nominal diameters of mooring lines while its coefficient of variation can be assumed as 0.1 [56].

In summary, the resistances of r_b, r_t and r_m are modelled as random variables whose statistics are explicitly provided. Given these stochastic resistance models and the ultimate loads, the failure probability of the OC4-DeepCwind semisubmersible can be estimated according to equation (9) as,

$$P = P[G(r_b, S_b) \le 0 \mid G(r_t, M_t) \le 0 \mid G(r_m, T) \le 0] \quad (9)$$

Equation (9) implies that the offshore wind turbine fails if one of the three critical components (blade, tower and mooring line) fails. Based on the simulated loads and modelled resistances, the failure probability of the OC4-DeepCwind in the China coastal waters is calculated and presented in Fig. 7.

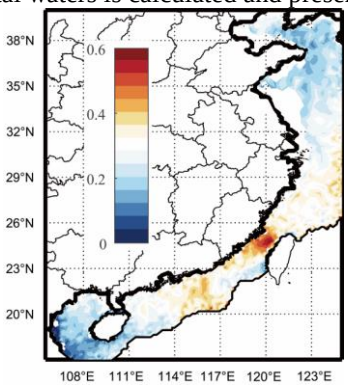

Fig. 7 Failure probability of the OC4-DeepCwind semisubmersible wind turbine in the China coastal waters.

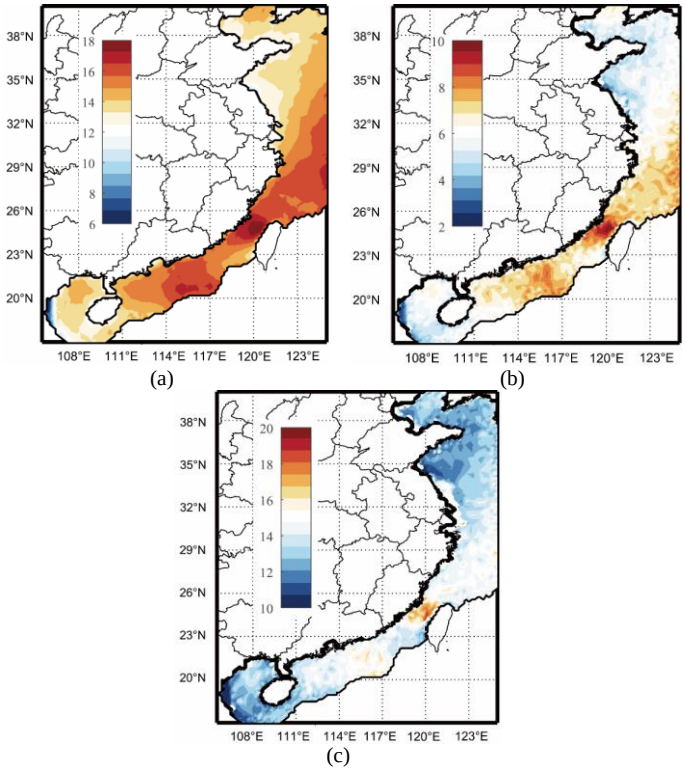

Fig. 8 Mean of the simulated extreme wind and wave fields. (a) Extreme wind speeds at 90m (unite: m/s). (b) Extreme significant wave height (unite: m). (c) Extreme spectral peak period (unite: s).

From Fig. 7, it is found that the maximum failure probability, which is around 0.6, has been found in Taiwan Strait where the maximum value of extreme wind speeds and wave heights are also observed as indicated in Fig. 8. The failure probability in the South China Sea and the East China Sea is around 0.3-0.45. The mean of the extreme wind speeds and wave heights in such areas are found less than in Taiwan Strait by ~12.50%, which implies that the decreases in extreme wind speeds and wave heights and the reductions in the failure probability are not linearly related. In other words, the spatial variations in failure probabilities can not be reliably estimated based solely on the extreme wind and wave fields, and the interactions between winds/waves and floating foundations are important in the estimation of failure probabilities.

C. Point failure probability

With the purpose of further discussing the failure probability of the OC4-DeepCwind floating wind turbine, 4 typical locations in different sea areas are selected where the ultimate loads and resistances in different parts of the floating wind turbines are discussed in details. The longitudes, latitudes and other relevant information on the selected locations are listed in Table VIII.

TABLE VIII

COORDINATES OF THE SELECTED 4 TYPICAL LOCATIONS IN CHINA COASTAL WATERS.

Location	Longitude ° E	Latitude ° N	Water depth (m)	Distance off the coast (km)	Sea areas
A	119.45	24.92	34.23	32.34	Taiwan Strait 1
B	120.86	25.03	68.66	115.82	Taiwan Strait 2
C	124.80	38.30	22.02	243.25	Bohai Gulf

D	115.03	20.46	150.74	217.29	The South China Sea

Fig. 9 shows box-whisker plots illustrating the dispersals in our dataset concerning the ultimate loads and the resistances of blade root, tower base and mooring line at the selected locations.

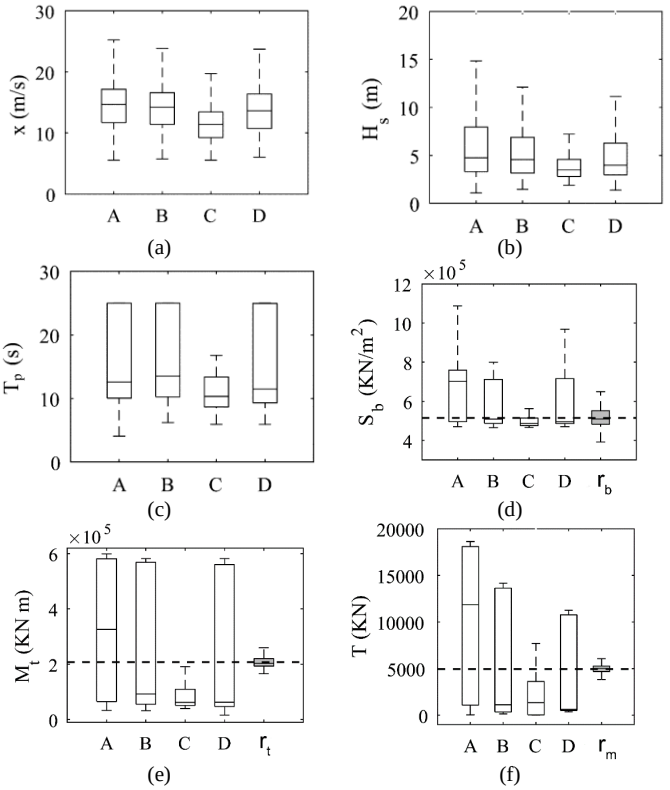

Fig. 9 Box-whisker plot of wind speed series at 10m x, significant wave height H_s, spectral peak period T_p, flapwise bending stress at the blade root S_b, tower base bending moment M_t, the mooring line tensions T and the resistances (r_b, r_t and r_m). The dashed line represents the mean of the resistances.

The dispersals, indicated by the Inter Quartile Range (IQR) of the box-whisker plot shown in Fig. 9, of the ultimate loads at the location C (Bohai Gulf) is less than other locations. Such an observation indicates that the sea state in Bohai Gulf is less influenced by typhoons and hence is stable. In particular, the high upper quartiles (Q3) corresponding to the locations A, B and D imply that the extreme wind and wave loads in the Taiwan Strait and South China Sea could be substantially higher than the mean values shown in Fig. 8, and consequently corresponds to a higher failure probability. Given that the IQR of the resistances of r_b, r_t and r_m are included in Fig. 9, the failure of the turbine can be illustrated through comparing the boxes of resistances to the boxes of loads. For example, the load boxes of M_t and T corresponding to the location A are found higher than the resistances boxes (2.08×10^5KN m for r_t and 4.95×10^3KN for r_m), which implies that the structural failure can be largely attributed to the failure of the tower base and the mooring lines. In addition to the box-whisker plots of the data, all the failure probabilities of the offshore wind turbines and the associated wind speeds, significant wave heights, spectral peak periods and the simulated ultimate loads are listed in Table IX.

TABLE IX

FAILURE PROBABILITY FOR OFFSHORE WIND TURBINES AT SELECTED 4 LOCATIONS. (x_{10} IS THE MEAN OF THE EXTREME WIND SPEED SERIES AT 10M. P_s, P_M AND P_T ARE THE FAILURE PROBABILITY FOR S_b, M_t AND T. P IS THE COMPREHENSIVE FAILURE PROBABILITY).

Index	A	B	C	D	Resistance
x_{10} (m/s)	14.73	14.31	11.80	14.27	-
H_s (m)	9.48	7.81	5.27	6.93	-
T_p (s)	16.23	17.15	12.06	14.71	-
$S_b \times 10^5$ (KN/m^2)	6.34	5.84	5.30	5.81	5.18
$M_t \times 10^5$ (KN · m)	3.28	2.46	1.46	2.09	2.08
$T \times 10^3$ (KN)	9.82	5.31	4.24	3.64	4.95
P_S	0.53	0.34	0.16	0.29	-
P_M	0.52	0.36	0.16	0.30	-
P_T	0.52	0.35	0.21	0.29	-
P	0.55	0.37	0.23	0.32	-

It is evident that the structural failure at the locations A, B and D could be resulted from the failures in any of the three critical parts or their combination. The failure at the location C, on the other hand, is dominated by the mooring line break due to the fact that P_T is much larger than P_S and P_M. From Table IX, it is found that even though the mean of extreme wind speed series at the locations A, B and D are similar, not only the failure probabilities of the critical parts (P_s, P_M and P_T) but also the comprehensive failure probability (P) at location A is much larger than at the other two locations. One plausible explanation might be that the probability density distributions of the ultimate loads are different at the location A and at the locations of B and D in spite of the similar mean, as shown in Fig. 10.

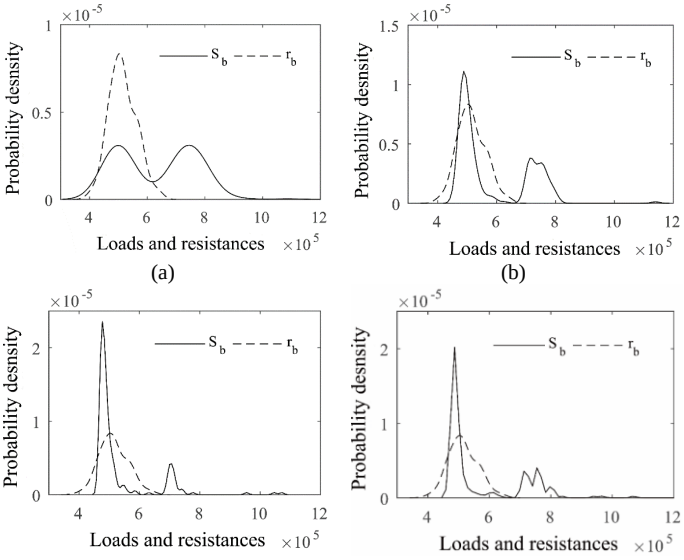

Fig. 10 Probability densities of S_b and r_b at locations A-D (Unite: KN/m^2). (a) Location A. (b) Location B. (c) Location C. (d) Location D.

From Fig. 10, it is evident that the probability density distributions of the ultimate loads are bimodal, which are not revealed by the mean presented in Table IX. The first peaks are found close to the concentrations of the probability distribution corresponding to r_b. Consequently, the second peaks contribute to the failure of the turbine because the chance for the resistance (r_b) exceeding the second peak is slim. In addition, Fig.10 implies that the turbine blade at the location A has higher chance to fail as the second peak in Fig. 10(a) is broader than in Fig. 10(b-d). Other ultimate load probability density distributions, such as the M_t and T,

This article has been accepted for publication in a future issue of this journal, but has not been fully edited. Content may change prior to final publication. Citation information: DOI 10.1109/TSTE.2018.2834471, IEEE Transactions on Sustainable Energy

sharing similar variation patterns are presented in Fig. 11 for references.

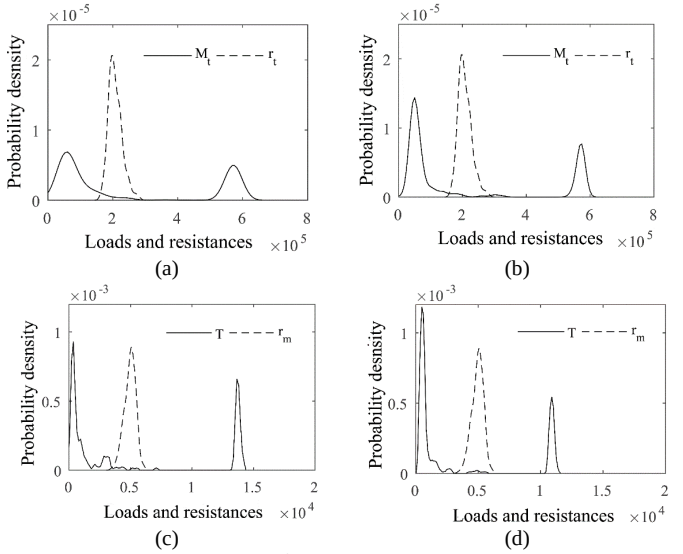

Fig. 11 Probability densities of the ultimate loads and resistances at location B and D. (a) M_t and r_t at location B (unite: KN· m). (b) M_t and r_t at location D (unite: KN· m). (c) T and r_m at location B (unite: KN). (d) T and r_m at location D (unite: KN).

In general, the probability distributions of M_t and T are bimodal, which are similar with the distribution of S_b, as shown in Fig. 11. In addition, the first peaks of M_t and T are different from those of S_b in terms of showing the value quite smaller than the resistances (r_t and r_m). Such finding indicates that the second peaks observed in the probability density distributions corresponding to the ultimate loads (M_t and T) determine, to a large extent, the failure probability of the tower base and the mooring lines. The bimodal distributions shown in Figs. 10 and 11 imply that the extreme wind and wave loads simultaneously influence the mooring line tensions and the buckling moments at the blade rotor and tower base. The combination of the extreme winds and waves make the ultimate loads concentrated on two major probability intervals. In other word, the bimodal probability distributions shown in Figs. 10 and 11 indicate that the ultimate loads in the three critical parts of the floating wind turbine are not in a linear relationship with the extreme winds and waves.

V. Conclusion remarks

In present study, a numerical framework is articulated, which couples the meteorology simulation, dynamics simulation and damage model to predict the failure probability of the OC4-DeepCwind offshore wind turbine in the China coastal waters.

Based on the simulation results, the failure probability of a site-specific wind turbine is estimated by checking the maximum ultimate loads acting on the three critical parts of the floating wind turbine against the resistances. Take the OC4-DeepCwind semisubmersible as an example, the area-wide and point failure probability predictions are derived from comparing the ultimate loads acting on the blade root, tower base and mooring line to the structural resistance. It is found that the maximum failure probability (~0.6) occurs in Taiwan Strait where the maximum values of extreme wind speeds and significant wave heights are also observed. Moreover, the failure probability in the South China Sea and the East China Sea is around 0.3-0.45 due to the influence of the numerous typhoons. Although the failure probability is connected to the intensity of the extreme wind and wave fields, the assessment of the failure of the offshore wind turbine relies heavily on the interactions between the wind turbine and the extreme wind/wave environment. Such a conclusion is substantiated by the point failure probability predictions. More specifically, the bimodal probability density distributions of the ultimate loads reveal that ultimate loads, and hence the failure probability, are not in a simple linear relationship with the extreme wind speeds and wave heights/periods.

References

[1] Li W, Yao H, Wang H, Wang Z. Latest development status of offshore wind power in China—The perspective of developers. Journal of Renewable & Sustainable Energy. 2014;6:786-803.
[2] Hong L, Möller B. Feasibility study of China's offshore wind target by 2020. Energy. 2012;48:268-77.
[3] Liu Y, Li S, Chan PW, Chen D. Empirical correction ratio and scale factor to project the extreme wind speed profile for offshore wind energy exploitation. IEEE Transactions on Sustainable Energy. 2017;PP:1.
[4] Hong L, Möller B. Risks of tropical cyclones on offshore wind farms in China. 6th Dubrovnik Conference on Sustainable Development of Energy, Water and Environment Systems. 2011.
[5] Madsen HO, Krenk S, Lind NC. Methods of Structural Safety: Prentice-Hall, Inc; 1986.
[6] Ronold KO, Larsen GC. Reliability-based design of wind-turbine rotor blades against failure in ultimate loading. Engineering Structures. 2000;22:565-74.
[7] Toft HS, Sørensen JD. Stochastic Models for Strength of Wind Turbine Blades using Tests. European Wind Energy Association. 2008.
[8] Toft HS, Sørensen JD. Reliability-based design of wind turbine blades. Structural Safety. 2011;33:333-42.
[9] Sørensen JD, Tarp-Johansen NJ. Reliability-based optimization and optimal reliability level of offshore wind turbines. International Journal of Offshore & Polar Engineering. 2005;15:141-6.
[10] Rose S, Jaramillo P, Small MJ, Grossmann I, Apt J. Quantifying the hurricane risk to offshore wind turbines. Proceedings of the National Academy of Sciences of the United States of America. 2012;109:3247-52.
[11] Garciano LEO, Koike T. New Reference Wind Speed for Wind Turbines in Typhoon-Prone Areas in the Philippines. Journal of Structural Engineering. 2010;136:463-7.
[12] Luo Y, Ahilan R. Mooring Safety Assessment Using Reliability Techniques. Moorings. 1991.
[13] Larsen K, Mathisen J. Reliability-based mooring design for a drilling semisubmersible. Proc of ISOPE conference1996. p. 457-66.
[14] Vazquez-Hernandez AO, Ellwanger GB, Sagrilo LVS. Reliability-based comparative study for mooring lines design criteria. Applied Ocean Research. 2006;28:398-406.
[15] Montes-Iturrizaga R, Heredia-Zavoni E, Silva-González F. On the estimation of mooring line characteristic resistance for reliability analysis. Applied Ocean Research. 2007;29:239-41.
[16] Jiang D, Zhuang D, Huang Y, Wang J, Fu J. Evaluating the spatio-temporal variation of China's offshore wind resources based on remotely sensed wind field data. Renewable & Sustainable Energy Reviews. 2013;24:142-8.
[17] Jha A, Dolan D, Musial W, Smith C. On Hurricane Risk to Offshore Wind Turbines in US Waters. Offshore Technology Conference2010.
[18] Bayati I, Gueydon S, Belloli M. Study of the Effect of Water Depth on Potential Flow Solution of the OC4 Semisubmersible Floating Offshore Wind Turbine. Energy Procedia. 2015;80:168-76.
[19] Grell GA, Peckham SE, Schmitz R, McKeen SA, Frost G, Skamarock WC, et al. Fully coupled "online" chemistry within the WRF model. Atmospheric Environment. 2005;39:6957-75.
[20] Michalakes J, Dudhia J, Gill D, Klemp J, Skamarock W. Design of a next-generation regional weather research and forecast model. Towards teracomputing. 1998:117-24.
[21] Liu Y, Chen D, Li S, Chan PW. Revised power-law model to estimate the vertical variations of extreme wind speeds in China coastal regions. Journal of Wind Engineering and Industrial Aerodynamics. 2018;173:227-40.

[22] Carvalho D, Rocha A, Gómez-Gesteira M. Ocean surface wind simulation forced by different reanalyses: Comparison with observed data along the Iberian Peninsula coast. Ocean Modelling. 2012;56:31-42.
[23] Davis CA, Low-Nam S. The NCAR-AFWA Tropical Cyclone Bogussing Scheme. Nam. 2001.
[24] Bouyé E, Durrleman V, Nikeghbali A, Riboulet G, Roncalli T. Copulas for Finance - A Reading Guide and Some Applications. Ssrn Electronic Journal. 2000.
[25] Chang CM, Fang HM, Chen YW, Chuang SH. Discussion on the Maximum Storm Radius Equations When Calculating Typhoon Waves. Journal of Marine Science & Technology. 2015;23.
[26] Laprise R. The Euler equations of motion with hydrostatic pressure as an independent variable. Monthly weather review. 1992;120:197-207.
[27] Paulson CA. The mathematical representation of wind speed and temperature profiles in the unstable atmospheric surface layer. Journal of Applied Meteorology. 1970;9:857-61.
[28] Skamarock WC, Klemp JB, Dudhia J, Gill DO, Barker DM, Wang W, et al. A Description of the Advanced Research WRF Version 3. 2008. p. 7--25.
[29] Hong S-Y, Pan H-L. Nonlocal boundary layer vertical diffusion in a medium-range forecast model. Monthly weather review. 1996;124:2322-39.
[30] Dudhia J. A Multi-layer Soil Temperature Model for MM5. Psu/ncar Mesoscale Model Users' Workshop1996.
[31] Kain JS. The Kain-Fritsch convective parameterization: an update. Journal of Applied Meteorology. 2004;43:170-81.
[32] Hong S-Y, Dudhia J, Chen S-H. A revised approach to ice microphysical processes for the bulk parameterization of clouds and precipitation. Monthly Weather Review. 2004;132:103-20.
[33] Mlawer EJ, Taubman SJ, Brown PD, Iacono MJ, Clough SA. Radiative transfer for inhomogeneous atmospheres: RRTM, a validated correlated‐k model for the longwave. Journal of Geophysical Research: Atmospheres (1984–2012). 1997;102:16663-82.
[34] Pollard RT, Rhines PB, Thompson RORY. The deepening of the wind-Mixed layer. Geophysical Fluid Dynamics. 1972;4:381-404.
[35] Mckinley S, Levine M. Cubic Spline Interpolation. Numermathjchinese Univ. 1999;64:44-56.
[36] Li SH, Hong HP. Typhoon wind hazard estimation for China using an empirical track model. Natural Hazards. 2016;82:1009-29.
[37] Fisher RA, Tippett LHC. Limiting forms of the frequency distribution of the largest or smallest member of a sample. Mathematical Proceedings of the Cambridge Philosophical Society. 1928;24:180-90.
[38] Cam LL. Maximum likelihood: An introduction. International Statistical Review. 1990;58:153--71.
[39] Teng, Liu PC. Estimating Wave Height Distributions from Wind Speed Distributions. Internationa Conference on Coastal Engineering2000.
[40] Isaacson MDSQ, Mackenzie NG. Long-term distributions of ocean waves: a review. Journal of the Waterway Port Coastal & Ocean Division. 1981;107:93-109.
[41] Moan T, Gao Z, Ayala-Uraga E. Uncertainty of wave-induced response of marine structures due to long-term variation of extratropical wave conditions. Marine Structures. 2005;18:359-82.
[42] Myrhaug D, Fouques S. A joint distribution of significant wave height and characteristic surf parameter. Coastal Engineering. 2010;57:948-52.
[43] Jonkman JM, Buhl ML. FAST User's Guide SciTech Connect: FAST User's Guide. 2005.
[44] Sørensen JD, Toft HS. Probabilistic Design of Wind Turbines. Energies. 2010;3:241-57.
[45] Bayati I, Gueydon S, Belloli M. Study of the Effect of Water Depth on Potential Flow Solution of the OC4 Semisubmersible Floating Offshore Wind Turbine. Energy Procedia. 2015;80:168-76.
[46] Robertson A, Jonkman J, Masciola M, Song H, Goupee A, Coulling A, et al. Definition of the Semisubmersible Floating System for Phase II of OC4. Scitech Connect Definition of the Floating System for Phase IV of Oc3. 2014.
[47] Hasselmann K, Barnett T, Bouws E, Carlson H, Cartwright D, Enke K, et al. Measurements of wind-wave growth and swell decay during the Joint North Sea Wave Project (JONSWAP). Deutches Hydrographisches Institut; 1973.
[48] Hall M, Goupee A. Validation of a lumped-mass mooring line model with DeepCwind semisubmersible model test data. Ocean Engineering. 2015;104:590-603.
[49] API. Recommended practice for design and analysis of stationkeeping systems for floating structures. 1995.
[50] Wang C, Jin S. Error features and their possible causes in simulated low-level winds by WRF at a wind farm. Wind Energy. 2013;17:1315–25.
[51] Carvalho D, Rocha A, Gómez-Gesteira M, Santos CS. WRF wind simulation and wind energy production estimates forced by different reanalyses: Comparison with observed data for Portugal. Applied Energy. 2014;117:116-26.
[52] Coulling AJ, Goupee AJ, Robertson AN, Jonkman JM, Dagher HJ. Validation of a FAST semi-submersible floating wind turbine numerical model with DeepCwind test data. Journal of Renewable and Sustainable Energy. 2013;5:023116.
[53] Tran TT, Kim DH. Fully coupled aero-hydrodynamic analysis of a semi-submersible FOWT using a dynamic fluid body interaction approach. Renewable Energy. 2016;92:244-61.
[54] Liu Y, Xiao Q, Incecik A, Peyrard C, Wan D. Establishing a fully coupled CFD analysis tool for floating offshore wind turbines. Renewable Energy. 2017;112:280-301.
[55] Ang HS, Tang WH. Probability Concepts in Engineering Planning and Design, Vol. II. Decision, Risk, and Reliability: Wiley; 1984.
[56] Kim H, Choung J, Jeon GY. Design of mooring lines of floating offshore wind turbine in Jeju offshore area. Journal of the Society of Naval Architects of Korea. 2014;9:V09ATA042-V09AT09A.

Yichao Liu received the B.S degree in marine technology from Dalian Maritime University, Dalian, China, 2014. He is currently a Ph.D. candidate in the School of Environment, Tsinghua University.

His research interests include the offshore wind energy and the numerical weather prediction.

Sunwei Li received the Ph.D degree in civil and environmental engineering department of the University of Western Ontario, Canada, 2012. From 2012-2014, he was a postdoctoral researcher in Hong Kong University of Science and Technology. He is currently an assistant professor in the Department of Ocean Science and Technology, Graduate School at Shenzhen, Tsinghua University.

His research interests include the renewable energy technologies, wind engineering and the numerical weather prediction.

P.W. Chan received the Master degree in Physics and mathematics from the University of Hong Kong, Hong Kong, China, 1994. He is currently a senior scientific officer of the Hong Kong Observatory.

He has been working on aviation weather service for nearly 20 years. He has contributed to the developments of the various low level wind shear and turbulence alerting algorithms of the Hong Kong International Airport. Recently he has been involved in a wake vortex detection programme at the airport. He has published various papers on meteorological applications.

Daoyi Chen received the Ph.D degree in Hydraulics and River Dynamics from the Tsinghua University, Beijing, China, 1988. From 2005-2011, he was a chair professor in the University of Liverpool. He is currently an academic leader (full professor) in the Department of the Ocean Science and Technology, Graduate School at Shenzhen, and the School of Environment, Tsinghua University.

He is one of the founders of the shallow water hydrodynamics and has published various papers on marine renewable and sustainable energy and the marine science and technology.